Arabian Journal of Geosciences (2022) 15: 169
https://doi.org/10.1007/s12517-021-09415-y

ORIGINAL PAPER

Zircon U–Pb dating and geological significance of the Dzhalinda intrusion in the Kirovskoe gold deposit, Russia

Baoyi Li[1] · Yanchen Yang[1] · Jianpeng Wang[1]

Received: 24 May 2021 / Accepted: 28 December 2021 / Published online: 15 January 2022

Abstract

The Dzhalinda intrusion is closely related to the mineralization of the Kirov gold deposit in the Far East of Russia. Based on the characterization of the petrology, geochemistry, and zircon U–Pb chronology of the Dzhalinda intrusion, this paper investigates the age, geochemical characteristics, and tectonic setting of the intrusion. The main rock is granodiorite. Petrological and geochemical analysis results show that the rocks have quartz (20%), potash feldspar (15%), plagioclase (60%), and biotite (3%), and belong to the calc-alkaline series. Trace element and rare earth element (REE) abundances suggest that the magma may primarily have originated from above the oceanic crust subduction of oceanic lithosphere mantle partial melting, wedge, and contamination by crustal material. Zircon U–Pb dating indicates that the Dzhalinda intrusion was formed in the Early Cretaceous, 125.44 ± 0.69 Ma. Combined with regional data, the Dzhalinda intrusion is considered to be formed by the subduction of the ancient Pacific plate with the Eurasische plate. Mineralization of the Kirovskoe gold deposit was the filling of the hydrothermal fluid along the NNE- and NW-trending faults following the magmatic period of the Dzhalinda intrusion.

Keywords Dzhalinda intrusion · Kirovskoe gold deposit · Paleo-Pacific Plate · Geochemical constrains · Geochronologic constrains

Introduction

The Kirovskoe gold deposit (54°47′N; 124°14′E) is located in the Shikinsko-Tukuringrskiy metallogenic belt in the Far East of Russia. An old mine with more than 80 years of mining history since1934, it is the source of placer gold from the largest gold deposit area in Russia's Far East—Relinda, Yang Na, and Ingagorin River Basin (to date, 217 tons of placer gold have been mined in this area) (Chai et al. 2017). The Shikinsko-Tukuringrskiy metallogenic belt is identified as one of the typical granite-related veined hydrothermal quartz-sulfide deposits of the gold-rare-metal type in East Russia (Gvozdev et al. 2020), and the lead-antimony-bismuth and telluride-bismuth mineralization is closely associated with the native gold (Bortnikov et al. 1982). The petrology (Abramov 2012), mineralogy (Gvozdev et al. 2013), metallogenic environment, and associated rare-metal ores (Gvozdev et al. 2020) of this belt have received significant attention during the last decades. The Dzhalinda intrusion, which is mostly composed of granodiorites and porphyry granites, hosts the main ore bodies in the southern part of the Kirovskoe deposit. Therefore, investigation of the genesis of the Dzhalinda intrusion is crucial to understanding the metallogenic mechanisms of the Kirovskoe deposit (Chai et al. 2017). The age of granodiorite intrusion and associated gold mineralization was determined to be 131–126 Ma using the Rb–Sr method (Chai et al. 2017) and 128–126 Ma using $^{40}Ar/^{39}Ar$ method (Sorokin et al. 2012) in Early Cretaceous. Despite this, the precise dating and the associated tectonic evolution of Dzhalinda intrusion are still lacking. Zircon U–Pb geochronology has the potential to improve the dating significantly (Armstrong-Altrin 2020). Also, the polygenous nature, formation duration, and the structural evolution of the gold deposits affect their economy significantly and are crucial to attempts to forecast and assess the distribution of the ore deposits. This paper aims to investigate the age and tectonic evolution of the genesis of

Responsible Editor: Domenico M. Doronzo

✉ Yanchen Yang
yyc@jlu.edu.cn

[1] College of Earth Sciences, Jilin University, 2199 Jianshe Street, Changchun 130021, China

Dzhalinda intrusion, using new geochronological and geochemical analyses including field observations, zircon U–Pb dating data, inorganic geochemical measurements to further improve understanding of the Shikinsko-Tukuringrskiy metallogenic belt, and the general gold deposit.

Geological setting and sample selections

Geological setting

The Kirovskoe deposit is located in the Siberian Craton, north of the Mongolia-Okhotsk Deep Fault (Fig. 1). The mining area is a graben, consisting of Middle Jurassic and Lower Cretaceous terrestrial sediments, along the east–west fault, with a length of 60 km and a maximum width of 6–7 km. The northern part is the Dzhalinda intrusion body, and the major rock types are granodiorite, biotite diorite, and diorite, covering an area of 50km^2. The fault structure is primarily near the east–west and northeast of the study area. The near east–west fault structure is a parallel secondary fault structure of Mongolia-Okhotsk deep fault that controls the formation and distribution of the graben.

The gold ore body is widely distributed near and inside the Dzhalinda intrusion body along the northern boundary of the graben (Fig. 1). The orebody surrounding rocks are composed mainly of Late Archean granite and granodiorite, as well as the Dzhalinda intrusion. The vein consists of diabase porphyry rock and has a close spatial relationship with the ore body. The ore body is a sulfide-quartz vein, and a few reticulated quartz zones and broken mineral zones. A total of about 500 orebodies were delineated, of which 31 orebodies were mined from 1934 to 1961. The thickness of the ore veins varies from 0.1–0.3 m to 3–4 m, and some ore bodies can be traced to 400–675 m along the strike. Along the trend, the ore bodies are as long as 350 m. The surrounding rock has been altered into greisen or fine-grain pyrite.

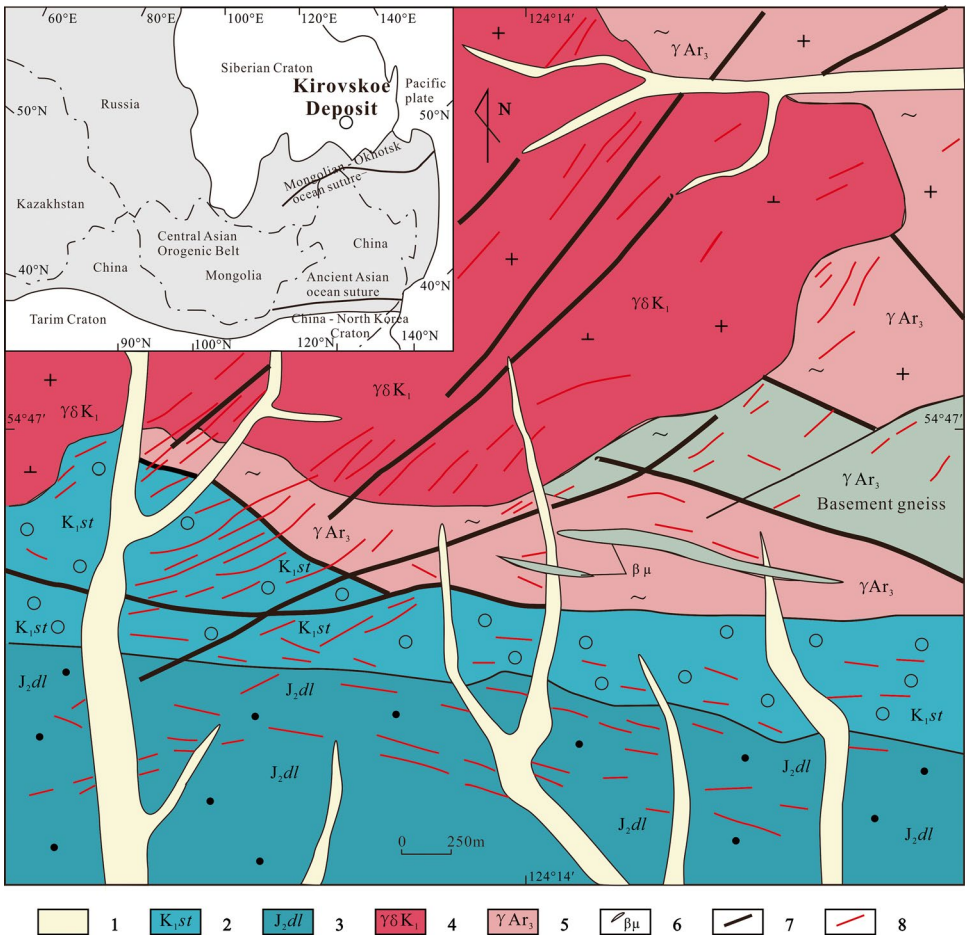

Fig. 1 Geological map of Kirovskoe deposit

1. Dikes; 2. Lower Cretaceous deposit; 3. Middle Jurassic deposit; 4. Early Cretaceous granodiorite; 5. Neoarchean granitic gneiss; 6. Diabase porphyry rock; 7 Faults; 8. Gold-bearing quartz vein.

The majority of the gangue minerals are quartz, with the remainder consisting of carbonate minerals, feldspar, and sericite. The quantity of ore minerals varies greatly, with pyrite, arsenian pyrite, bismuthite, chalcopyrite, and gold accounting for the majority. In contrast, sphalerite, galena, chalcopyrite, magnetite, sulfur-antimony lead ore, molybdenite, scheelite, and natural bismuth are rare. Natural gold has large particle sizes and commonly weighs between 10 and 15 g. Its relative purity is high with values of 844–977.

Gold is the main valuable element of this ore along with some other minor elements including silver, bismuth, copper, selenium, and tellurium. From 1934 to 1961, a total of 9,411 kg of gold ore was recovered from the Kirovskoe deposit, with an average grade of 8.5 g/t. Silver and copper are recovered alongside gold simultaneously.

From west to east, the Kirovskoe deposit can be divided into 5 mining sections: Yan-kan; Jinyuan; southern; central Dzhalinda; and Dzhagda. It is known that there are more than 300 large and small veins constituting the deposit, showing different formation temperatures, ranging from high to low. The combination of ore can be divided into six types (Gvozdev et al. 2013), and the purity of the gold gradually decreases. These include (1) Tourmaline-magnetite combination in the Yan-kan mine section, which was formed in broken hydrothermal altered surrounding rocks. In a few quartz veins, the main minerals are tourmaline and magnetite, and occasionally disseminated magnetite and pyrite. (2) Quartz combination: the main mineral is quartz, followed by pyrite and toxic sand, containing gold l-2 $\times 10^{-6}$ to 6×10^{-6}. (3) Bismuthite-chalcopyrite combination in the north-east veins at the intersection of the north-east and near east–west fissure zones. The main minerals are quartz, scheelite, magnetite, pyrite, chalcopyrite, bismuthite, and tellurite bismuthite. These contain gold from trace amounts to 100×10^{-6}, the relative purity of gold is higher, 920–940, and the gold particles are larger. (4) Pyrite-poison sand combination with the main minerals quartz, pyrite, toxic sand, and cobaltite, containing gold 4–6×10^{-6} to 140×10^{-6}, the gold is in a dispersed state, and the relative purity is 850. (5) Polymetallic mineral combination in the near-westward veins with mainly quartz, iron dolomite, pyrite, chalcopyrite, galena, and toxic sand. The gold content ranges from trace amounts to 4–6×10^{-6}. 6) The latest quartz-antimony ore combination appears in the east–west ore veins in the east of the deposit, mainly chalcedony quartz, antimony ore, barite, calcite, and cinnabar, with a trace gold content of 2×10^{-6}.

Sample selection

A group of NW-oriented Au-Q-sulfide veins within the Early Cretaceous granodiorite saprolite body are discovered, and the mineralization is often in contact with the Dzhalinda granodiorite wall with distinct boundaries. The Dzhalinda granodiorite and surrounding rocks were therefore selected in this study to investigate the metallogenic age of the deposit. Six samples of the host rocks were selected for petrology, major, trace, and REE analyses. Based on the geochemical analysis, two samples were selected to conduct zircon U–Pb dating for geochronologic analysis.

Analytical methods

Major and trace element analyses

The main elements and trace elements were analyzed for all 6 samples. The analysis and testing work were completed at the Experimental Test Centre, Xi'an Institute of Geology and Mineral Resources (Tables 1, 2, and 3). Specifically, the main elements were analyzed by X-ray fluorescence spectroscopy (XRF), with the analysis accuracy better than 1%. The rare earth and trace elements were measured by SX-2 inductively coupled plasma mass spectrometer (ICP-MS), and the analysis accuracy was better than 5 ~ 10%.

Zircon U–Pb dating

One sample from Dzhalinda intrusion and one sample from the surrounding gneissose granite were selected for geochronologic analysis to quantify the ages of the orebody and the crystalline basement of the ore field. Twenty zircon grains were tested in each sample for U–PB dating.

Geochronologic analysis was conducted using zircon U–Pb dating, which consists of two stages. First, the zircon grains were obtained in cathode luminescence (CL) with a cathode luminometer loaded with an electronic probe instrument at the State Key Laboratory of Continental Dynamics, Northwest University, China. Subsequently, LA-MC-ICP-MS zircon U–Pb annual test analysis was completed using Finnigan Neptune MC-ICP-MS and the Newwave UP 213 Laser ablation system at the MCICP-MS laboratory of the Institute of Mineral Resources, Chinese Academy of Geological Sciences, China.

The diameter of the spot beam used for laser ablation was 25 μm, with He as the carrier gas. Dating accuracy and accuracy of the zircon standard was about 1% (2σ). The zircon U–Pb dating used zircon GJ-1 as the external standard, and the U and Th content used zircon M127 (U: 923×10^{-6}; Th: 439×10^{-6}; Th/U: 0.475) for external standard correction (Nasdala et al. 2008; Sláma et al. 2008). During the test, two zircons GJ-1 were repeatedly measured before and after every 5–7 samples to calibrate the samples (Table 4). A zircon plesovice was measured and the state of the instrument was observed to ensure the accuracy of the test. The data were processed using the ICPMSDataCal program, and the zircon age harmony map was obtained using the Isoplot 3.0

Table 1 Main elements results of 6 selected samples

Sample	Oxide content ($\times 10^{-2}$)														Indexes				
	SiO_2	TiO_2	Al_2O_3	Fe_2O_3	FeO	MnO	MgO	CaO	Na_2O	K_2O	P_2O_5	H_2O^+	∑	DI		A/NK	A/CNK	δ	A.R
A	68.50	0.35	16.34	0.85	1.71	0.09	1.15	4.27	4.57	1.57	0.15	0.26	99.80	72.8		1.76	0.96	1.48	1.85
B	63.44	0.65	14.36	1.08	3.80	0.10	4.29	4.83	3.21	3.53	0.20	0.30	99.79	62.6		1.58	0.81	2.02	2.00
C	65.86	0.56	17.12	0.88	1.48	0.07	1.59	4.40	4.94	2.18	0.21	0.47	99.75	72.35		1.63	0.93	2.22	1.99
D	62.20	0.68	15.45	1.54	3.45	0.11	3.98	5.22	3.73	2.95	0.21	0.23	99.75	61.62		1.66	0.82	2.32	1.96
E	72.10	0.08	16.00	0.28	0.61	0.03	0.26	2.64	4.50	2.59	0.03	0.63	99.76	83.24		1.57	1.07	1.73	2.23
F	53.48	0.80	12.80	1.36	7.12	0.15	11.33	7.50	2.14	2.15	0.19	0.73	99.75	30.95		2.17	0.66	1.76	1.54

Table 2 Rare earth elements results of 6 selected samples

Sample	$\times 10^{-6}$															Indexes					
	La	Ce	Pr	Nd	Sm	Eu	Gd	Tb	Dy	Ho	Er	Tm	Yb	Lu	Y	∑ude	LR/HR	δEu	δCe	La/Yb	Sm/Nd
A	18.0	37.3	4.76	19.33	3.95	1.16	3.63	0.6	3.29	0.65	1.92	0.29	2.03	0.29	16.93	114.18	6.65	0.92	0.95	8.9	0.2
B	22.9	49.6	6.17	23.81	4.26	1.22	3.46	0.5	2.36	0.43	1.24	0.20	1.24	0.17	11.65	129.22	11.26	0.95	0.99	18.47	0.18
C	23.7	44.7	5.75	21.00	3.69	1.24	3.07	0.5	2.47	0.49	1.45	0.24	1.69	0.26	13.80	123.99	9.85	1.09	0.9	14.03	0.18
D	35.5	81.2	10.23	39.23	6.18	1.78	5.29	0.8	3.85	0.76	2.19	0.32	2.13	0.31	19.54	209.24	11.15	0.93	1.01	16.64	0.16
E	29.6	59.0	7.06	26.51	4.66	1.21	3.82	0.6	2.73	0.51	1.41	0.22	1.38	0.21	13.72	152.55	11.8	0.85	0.95	21.45	0.18
F	15.1	23.7	2.43	7.87	1.00	0.75	0.84	0.1	0.54	0.11	0.34	0.05	0.37	0.05	3.06	56.29	20.92	2.46	0.86	40.98	0.13
Chondrite*	0.310	0.808	0.122	0.600	0.195	0.073	0.259	0.047	0.322	0.072	0.210	0.032	0.209	0.032		1.000					

*(Boynton 1984)

Table 3 Trace elements results of 6 selected samples

Sample	$\times 10^{-6}$																					$\times 10^{-9}$			
	Rb	Ba	Th	U	K	Ta	Nb	La	Ce	Sr	Nd	P	Hf	Zr	Sm	Ti	Tb	Y	Yb	W	Zn	As	Cu	Mo	Pb	Au	Ag	Hg
A	46.6	469.2	4.6	1.2	17,881.4	0.4	5.2	18.0	37.3	451.9	19.3	849.1	3.7	90.0	3.9	4767.7	0.6	16.9	2.0	0.51	148	8.0	21	23.3	4.1	4.0	44	17.9
B	80.5	1159.4	7.1	2.5	29,268.0	0.8	7.1	22.9	49.6	653.8	23.8	879.4	6.6	114.2	4.3	3912.3	0.5	11.6	1.2	1.32	63	2.1	17	7.1	16.6	1.9	52	6.5
C	35.0	703.2	6.0	1.1	13,052.4	1.4	8.1	23.7	44.7	578.9	21.0	649.7	4.7	90.6	3.7	2073.1	0.5	13.8	1.7	15.93	32	5.7	48	3.5	8.4	5.5	90	6.5
D	42.8	868.6	5.4	1.6	18,075.4	0.6	6.3	35.5	81.2	607.0	39.2	899.1	9.1	199.3	6.2	3348.4	0.8	19.5	2.1	53.13	26	2.7	26	6.2	6.2	1.4	68	8.7
E	77.6	730.6	8.7	2.7	24,493.6	0.5	8.0	29.6	59.0	652.2	26.5	916.3	9.6	161.6	4.7	4074.4	0.6	13.7	1.4	1.60	59	3.3	17	5.4	19.3	2.3	61	15.7
F	53.3	668.9	5.7	0.6	21,467.6	0.2	1.5	15.1	23.7	475.8	7.9	128.9	2.2	44.3	1.0	502.4	0.1	3.1	0.4	56.94	11	6.9	37	6.1	7.3	31.4	259	7.6
Primitive mantle**	0.86	7.56	0.096	0.027	252	0.043	0.62	0.71	1.9	23	1.29	90.4	0.35	11	0.385	1200	0.099	4.87	0.43	1*	72*	2.4*	35*	0.9*	1.5*	4*	0.07*	0.08*

**(Wood et al. 1979) *Vickers value (Vickers 1962); values of K, P, Ti are calculated from oxides

program. During the sample analysis, the analysis result of the plesovice standard sample as an unknown sample was 337 ± 2 Ma ($n = 12$, 2σ), which corresponds to the recommended age value 337.13 ± 0.37 Ma (2σ) (Sláma et al. 2008).

Results

Petrological analysis

Based on the petrological observation, these Dzhalinda rock samples have medium to fine grain sizes, monzonitic textures, and massive structures. The mineral particle sizes are generally 0.3 to 2.0 mm, and the mineral compositions consist mainly of quartz (20%), potash feldspar (15%), plagioclase (60%), and biotite (3%). The secondary minerals are magnetite, sphene, and zircon. Quartz mostly fills with other grains including xenomorphic granular. The grain size of potash feldspar is uneven, and the individual grains up to 6 mm are encapsulated with euhedral plagioclase to form a monzonitic texture. Ring structure was observed with andesine-labradorite. Potassium metasomatism and secondary alteration such as sericite and chlorite are observed.

Six samples were characterized as below (Fig. 2):

Sample A: Granodiorite. This sample is identified as granodiorite-Kirov quartz vein type gold-rare metal deposit of the ore body and belongs to the second phase of the Upper Amur Early Cretaceous intrusive miscellaneous rocks.

Sample B: Gneissic granite. This type of rock is forming the crystalline base of the ore field and is a late Stanoff subalkaline granite miscellaneous rocks, presumed to be early Archean.

Sample C: Coarse porphyritic granodiorite porphyry. This type of rock is forming the granodiorite porphyry wall. Gold occurrences in the mining area, with leaching-like mineralization, which belongs to the late Jurassic Geocan subalkaline granite miscellaneous rocks.

Sample D: Alkaline granite miscellaneous rocks. These rocks are identified as coarse porphyritic granite, belonging to the late Jurassic geocan subalkaline granite miscellaneous rocks coarse porphyritic granite and constituting a large rock body.

Sample E: Gneissic granodiorite. It is forming the crystalline base, and the late Stanoff subalkaline granodiorite detrital, presumably early metasedimentary:

Sample F: Oblique hornblende gneiss. It forms the crystalline basement of regional metamorphic rocks.

All six samples were also classified by the QAP diagram of intrusive rocks according to the results of petrographic analysis (Fig. 3). They fell into grano-diorite (A), quartz

Table 4 Zircon U–Pb isotopic analysis results of selected granodiorite in Dzhalinda intrusion (sample A)

Sample	Isotopes Age/Ma												
	Th/U	$^{207}Pb/^{206}Pb$	1σ	$^{207}Pb/^{235}U$	1σ	$^{206}Pb/^{238}U$	1σ	$^{207}Pb/^{206}Pb$	1σ	$^{207}Pb/^{235}U$	1σ	$^{206}Pb/^{238}U$	1σ
D-01	1.17	0.0512	0.0019	0.1382	0.00523	0.01958	0.00018	250	70	131	5	125	1
D-02	1.24	0.0466	0.00201	0.12534	0.00556	0.01958	0.00021	29	75	120	5	125	1
D-03	1.27	0.05054	0.0041	0.14594	0.01147	0.02094	0.00042	220	185	138	10	134	3
D-04	1.11	0.0503	0.00187	0.1364	0.00534	0.0196	0.00023	209	69	130	5	125	1
D-05	1.04	0.05789	0.00209	0.1758	0.00757	0.02203	0.00062	526	48	164	7	141	4
D-06	1.37	0.04774	0. 00,283	0.12766	0.00734	0.0194	0.00028	86	132	122	7	124	2
D-07	1.07	0.05011	0.00351	0.13452	0.00923	0.01947	0.00029	200	160	128	8	124	2
D-08*	1.21	0.11894	0.02256	2.55656	0.43247	0.15589	0.01338	1940	370	1288	123	934	75
D-09	1.57	0.0505	0.00371	0.16296	0.01179	0.0234	0.00031	218	168	153	10	149	2
D-10	1.3	0.05355	0.00224	0.14285	0.00596	0.01958	0.00027	352	69	136	5	125	2
D-11	1.41	0.05845	0.00601	0.1608	0.01632	0.01995	0.00033	547	233	151	14	127	2
D-12	1.18	0.04793	0.00234	0.12996	0.00651	0.01962	0.00023	96	90	124	6	125	1
D-13*	2.36	0.04605	0.067	0.15622	0.22668	0.02461	0.00268		1522	147	199	157	17
D-14	2.16	0.05035	0.00297	0.13796	0.00785	0.01987	0.00031	211	137	131	7	127	2
D-15	1.43	0.04979	0.00189	0.13358	0.00507	0.01962	0.0002	185	69	127	5	125	1
D-16	1.52	0.05021	0.00459	0.15759	0.0139	0.02276	0.00054	205	208	149	12	145	3
D-17	1.48	0.05308	0.00167	0.14341	0.00467	0.01977	0.00026	332	50	136	4	126	2
D-18	1.61	0.05477	0.00529	0.15091	0.01436	0.01999	0.00034	403	221	143	13	128	2
D-19	1.58	0.06716	0.01759	0.18358	0.04139	0.01959	0.00046	843	455	171	36	125	3
D-20	1.6	0.05377	0.0072	0.14607	0.0195	0.0197	0.00021	361	303	138	17	126	1

Note: *means the sample is not shown in the Concordia diagram

monzonite (B), grano-diorite (C), grano-diorite (D), quartz monzodiorite/monzogabbro (E), and monzodiorite/monzogabbro (F) zones, respectively. Classification is essentially consistent with the field names.

Major elements

The five samples of the Dzhalinda rock mass have a similar SiO_2 content of 62.20 ~ 72.10%, with an average of 66.42%, which is acidly intermediate rock. Al_2O_3 content is 14.36 ~ 17.12%, with an average of 15.85%. MgO content is 0.26 ~ 11.33%, with an average of 2.25%. Na_2O content is 2.14 ~ 4.57%, with an average of 4.19% while K_2O content is 1.57 ~ 3.53%, with an average of 2.56%. Rittmann indexes ($\sigma = [\omega(K_2O + Na_2O)]^2/[\omega(SiO_2\text{-}43)]$ is 1.48 ~ 2.32, with an average of 1.93, > 1.8, < 3.3, which is calcium-alkaline. A/CNK ($= Al_2O_3/(CaO + Na_2O = K_2O)$ is 0.81 ~ 1.07, with an average of 0.875, which is an aluminum series (Clarke 1981). Differentiation index (DI) (the sum of the normative constituents Q + Ab + Or + Ne + Kp + Lc, where Q = quartz, Ab = albite, Or = orthoclase, Ne = nepheline, Kp = kaliophilite, and Lc = leucite) (Allaby 2013) is 61.62 ~ 83.24, with an average of 63.93.

The Dzhalinda intrusion consists of medium silicon, flat aluminum, and poor magnesium, which belongs to the medium potassium calcium basic series, with high sodium and low potassium. According to the diagram classification of type I and S granites (Chppell and White 1992; Fig. 3), all samples are type I granites.

In the R1-R2 granite tectonic environment discrimination diagram (Fig. 4), all points of samples in this study fall into zone 2 which is the area before the plate collision.

Trace elements

On the standardized cobweb map of trace element primitive mantle (Chondrite REE values from Boynton 1984; Fig. 5), it can be seen that the distribution curves of these elements are similar, which shows the characteristics of homology evolution (Fig. 6). Compared with the original mantle, it is slightly enriched in active incompatible elements such as the large ion philophile elements Rb, K, and Ba, while the high field strength elements such as Nb, Ta, Zr, P, Ti, are slightly depleted. The losses of Nb, Ta, Zr, and Sr may be related to the separation and crystallization of rutile, sphene, zircon, and plagioclase, respectively. The negative anomalies of P and Ti may be related to the separation and crystallization of apatite and ilmenite, indicating that they may have experienced a certain degree of fractional crystallization (DePaolo 1981).

From Table 1, compared with the average values of chemical elements in similar rocks in the Earth's crust

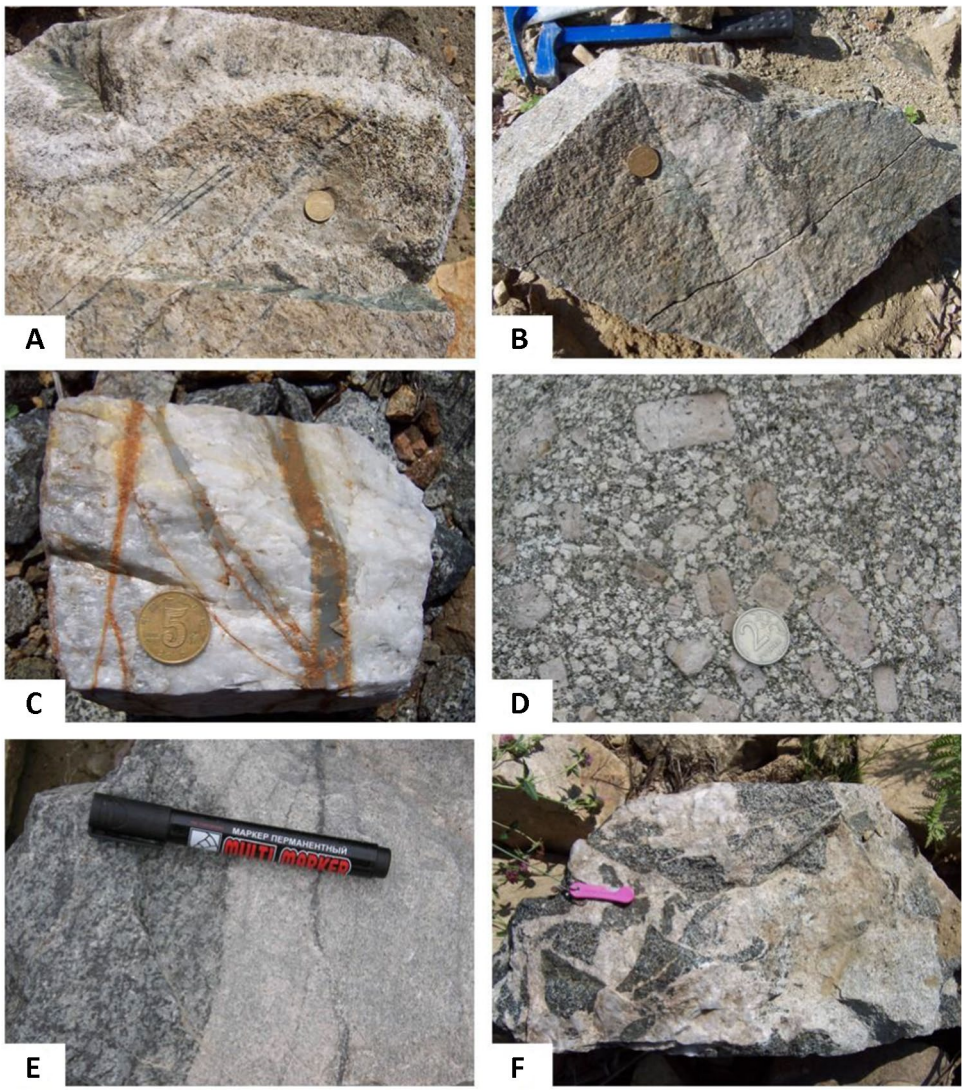

Fig. 2 Field photos of selected samples **A-F**. Sample **A**: granodiorite, sample **B**: gneissic granite, sample **C**: coarse porphyritic granodiorite porphyry wall, sample **D**: alkaline granite miscellaneous rocks coarse porphyritic granite, sample **E**: gneissic granodiorite, sample, **F**: oblique hornblende gneiss

(Vinogradov 1962; Yaroshevsky 2006), the Au, Ag, Cu, Pb, Zn, As, Hg, W, Mo elements of the Dzhalinda rock mass are all enriched to varying degrees, and the content is uneven. The dispersion coefficient is relatively great, and the high background value of the element promotes mineralization.

The total amount of REEs is $56.29\times10^{-6}\sim209.24\times10^{-6}$ in these samples, with an average value of 130.91×10^{-6}. The LR/HR value is 6.65 ~ 20.92, with an average value of 11.94, indicating that the fractionation of light and heavy rare earth is not obvious. The average value is 20.08; the Sm/Nd ratio is 0.13 ~ 0.2, and the average value is 0.17. According to the standardized distribution pattern diagram of REE chondrites (Fig. 7), the curves of these samples are very similar, with trends slightly inclined to the right, indicating that they belong to the type I granite. δEu value is 0.85 ~ 2.46, and the average value is 1.20. Eu has no negative anomalies, which also shows the characteristics of type I granite.

Zircon U–Pb dating

Stereomicroscopic observations and CL images (Fig. 8) show that the zircon in the granodiorite of Dzhalinda intrusions is light yellow, square bipyramidal, transparent, with a diamond-like luster. Some crystals have black mineral inclusions. The crystal plane and crystal edges are unclear. The length-to-width ratio is 2:1–3:1, and the particle size is 100–200 μm.

A total of 20 test points was conducted on the Dzhalinda granodiorite for the U–Pb dating results (Table 4). The Th/U ratio is all greater than 0.4, which shows the zircon is magmatic in origin [5, 6]. Among them, $^{206}Pb/^{238}U$ surface age values of C-08 and C-13 points are significantly higher. Combined with the CL observation (Fig. 8), the C-08 point is located in the core area in the secondary edge of a zircon grain. This indicates that the zircon is an early magmatic zircon captured by the rock body, and the surface age value

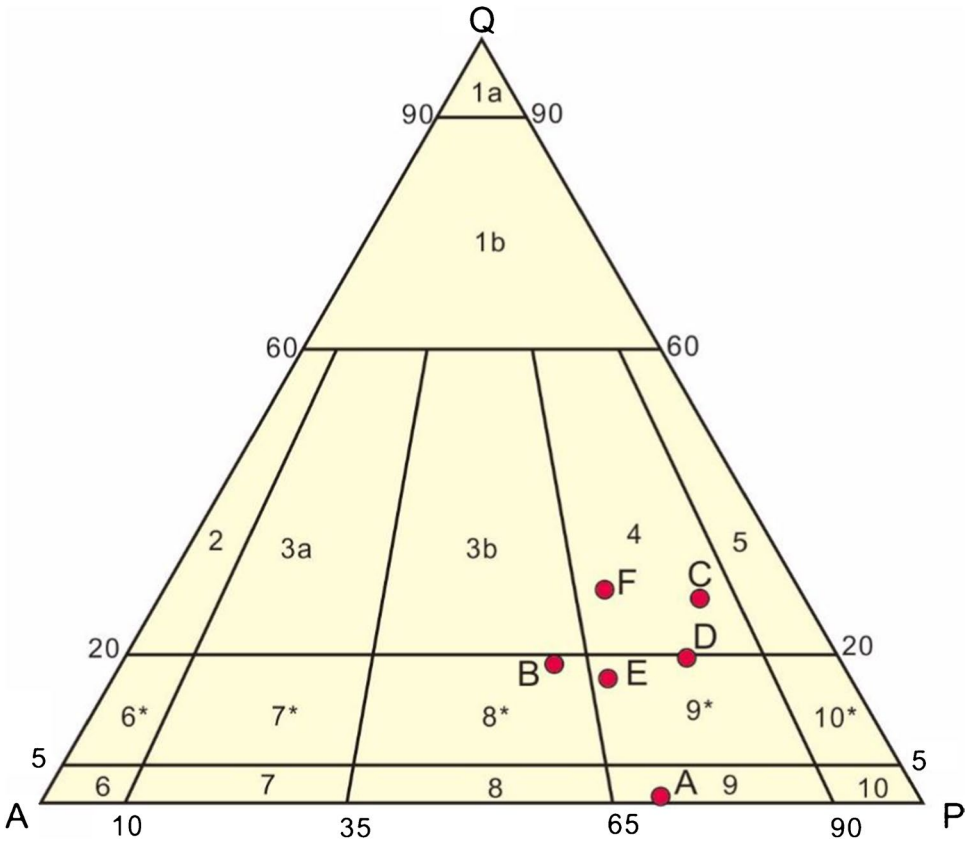

Fig. 3 QAP diagram of the Dzhalinda intrusive rocks. Q: quartz, A: alkali feldspar, P: plagioclase (modified after Streckeisen 1976). 1a, Quartzolite; 1b, quartz-rich granitoid; 2, alkali-feldspar granite; 3a, syeno-granite; 3b, monzo-granite; 4, grano-diorite; 5, tonalite; 6*, alkali-feldspar quartz syenite; 6, alkali-feldspar quartz syenite; 7*, quartz syenite; 7, syenite; 8*, quartz monzonite; 8, monzonite; 9*, quartz monzodiorite/monzogabbro; 9, monzodiorite/monzogabbro; 10*, quartz diorite/quartz gabbro; 10, diorite/gabbro

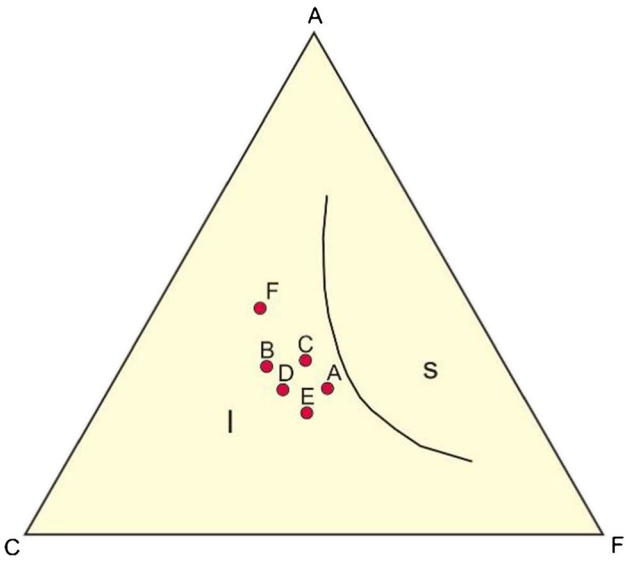

Fig. 4 ACF diagram of the Dzhalinda intrusive rocks (modified after Chppell and White 1992). A, Al_2O_3-Na_2O-K_2O; C, CaO; F, FeO + MgO; I, I-type granite; S, S-type granite

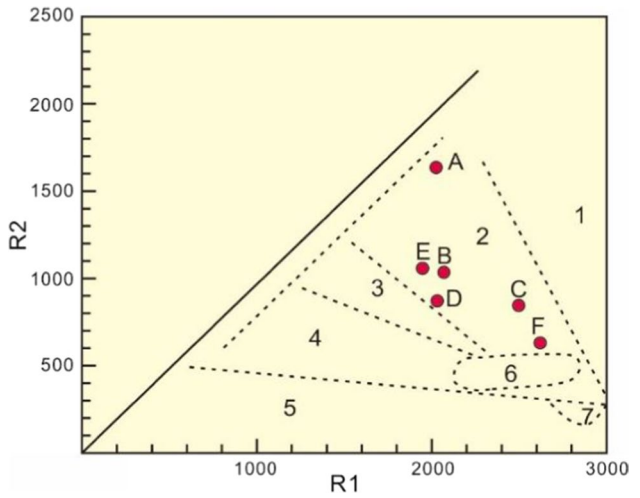

Fig. 5 R1-R2 multicationic diagram showing tectonic fields of the Dzhalinda intrusive rocks R1-4Si-11(K + Na)-2(Fe + Ti); R2-6Ca + 2 Mg + Al. 1, Mantle fractionates; 2, pre-plate collision; 3, post-collision uplift; 4, late-orogenic; 5, anorogenic; 6, syn-collision; 7, post-orogenic.

represents the age of the captured zircon. Point C-13 is located at the edge of a relatively broken zircon. Due to the fracture of the zircon surface at this point, and the destruction of the closed system, the radioactive cause of lead (uranium) was lost to a certain extent. The rest of the points are located at the edge of the relatively complete zircon. The measured $^{207}Pb/^{235}U$ and $^{206}Pb/^{238}U$ data are located in or near the U–Pb harmonic line, and the surface age value

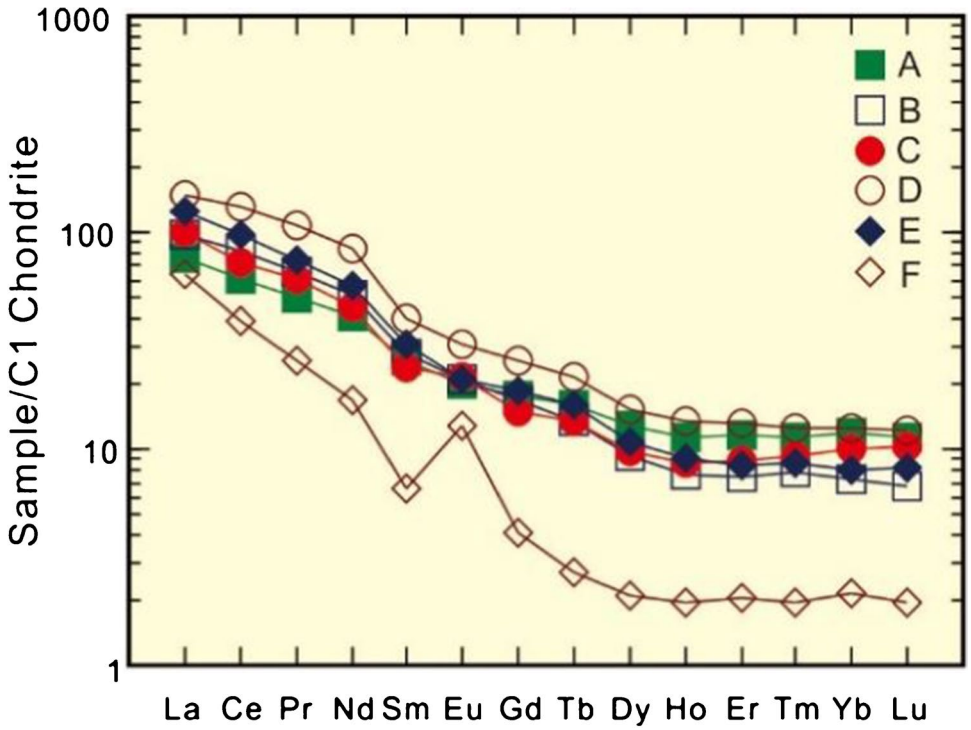

Fig. 6 Chondrite-normalized REE patterns of the Dzhalinda intrusive rocks (Chondrite REE values from Boynton 1984)

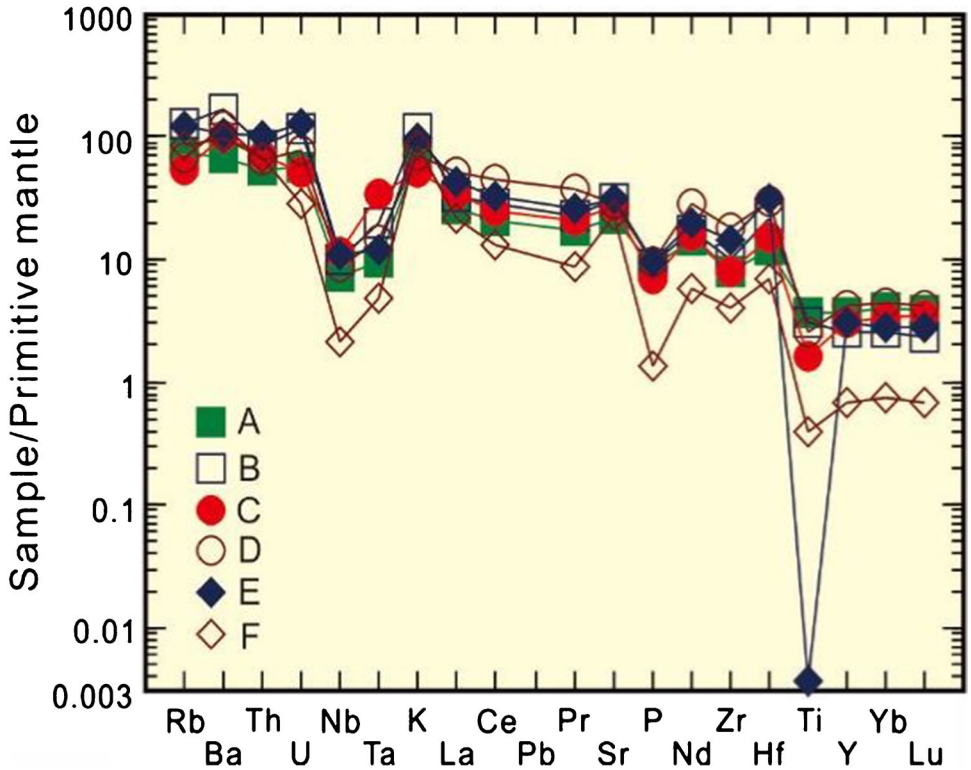

Fig. 7 Primitive mantle-normalized trace element spidergrams of the Dzhalinda intrusive rocks (Primitive mantlevalues from Sun and McDonough 1989)

of $^{206}Pb/^{238}U$ is between 125 and 149 Ma (Table 4). The weighted average age is 125.44 ± 0.69 Ma (Fig. 9), corresponding to the Early Cretaceous period. This represents the crystallization age of the magma.

A total of 20 test points was conducted on the surrounding gneissose granite for the U–Pb dating results to capture the age of the crystalline basement (Table 5, Fig. 10). Among them, 206Pb/238U surface age values of S-02 and

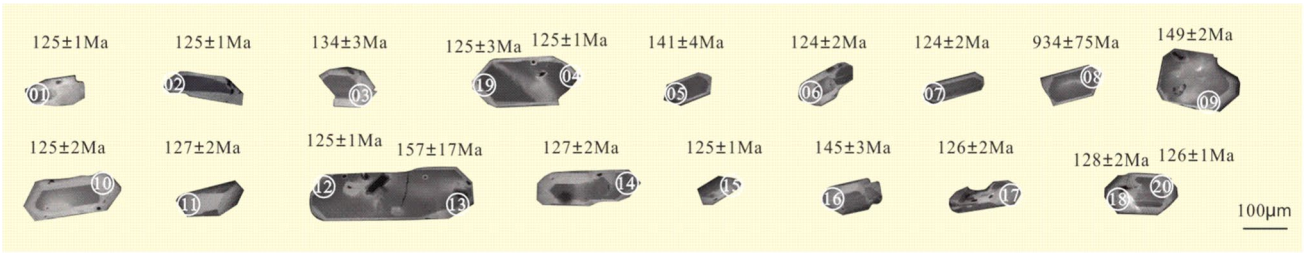

Fig. 8 Morphological and textual characterisation of zircon crystals in Dzhalinda granodiorite sample by CL images

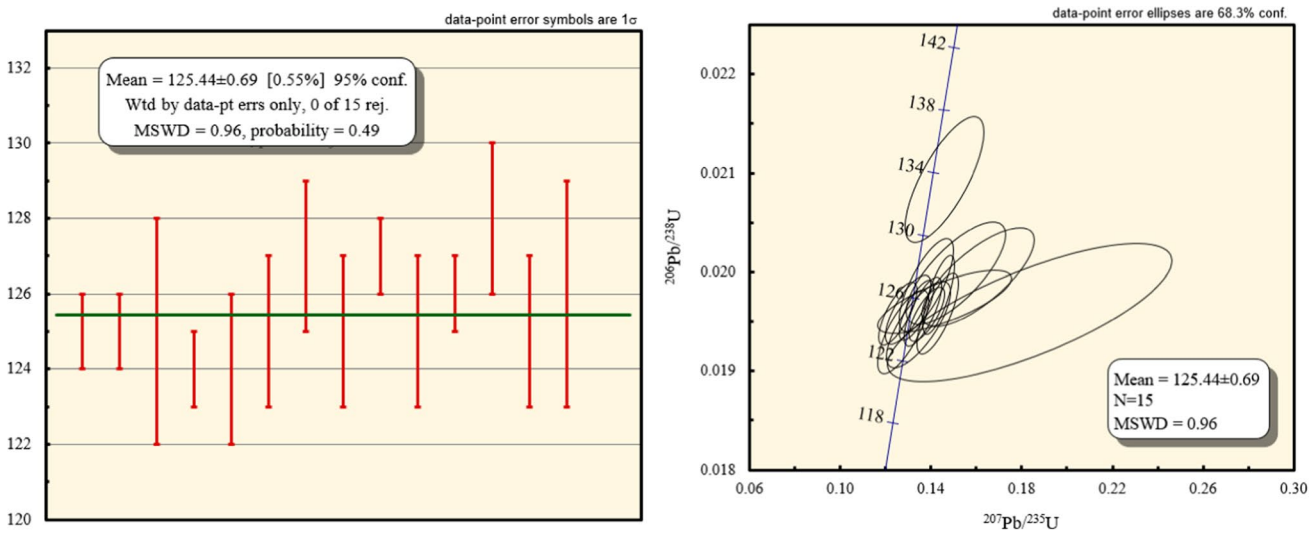

Fig. 9 Concordia diagram with U–Pb isotopic plots for zircons in Dzhalinda granodiorite sample

S-13 points are significantly higher and that of S-08 is significantly lower. Therefore, these three points were not considered in the dating analysis. The surface age values of $^{206}Pb/^{238}U$ in other samples are between 381 and 384 Ma (Table 5) with a weighted average age is 382.8 ± 1.2 Ma (Fig. 11), corresponding to the Late Devonian period.

Discussion

Based on the new geochemical, isotopic, and geochronological results obtained here, the following questions regarding the Dzhalinda intrusion in the Kirovskoe deposit are discussed: (1) the age and (2) the tectonic implications.

Gold mineralization age

The age of the Dzhalinda intrusion has been previously determined to be 131–126 Ma by Rb–Sr dating and 128–125 Ma by 40Ar/39Ar dating (Sorokin et al. 2014). In this study, the age has been identified as 125.44 ± 0.69 Ma (i.e., 124.75–126.13 Ma) by zircon U–Pb dating, which corresponds to the Early Cretaceous. This finding is consistent with previous studies using other dating methods, but the precision of the timing has been significantly improved in this study. The error of the age has been narrowed down from 4 to 1.38 MPa, and the range has reduced by 65.5%. The age of the Dzhalinda intrusion determined in this study further confirms that the granitoids intrusion occurred in stage three and the mineral composition is consisting of granodiorite, biotite diorite, and diorite during this stage. The Dzhalinda intrusion might be formed as a result of postmagmatic activity, and accompanied with coeval dikes. Also, the age of Dzhalinda intrusion is similar with massifs in the Tynda-Bakaran complex (Sorokin et al. 2014).

According to other studies, there are four stages of magmatism in the Kirovskoe deposit proposed in the previous research (e.g., Gvozdev et al. 2013): (1) Precambrian granite gneisses; (2) Paleozoic diorite porphyry and gabbroid dikes; (3) Early Cretaceous granitoids; and (4) Late Cretaceous Olekma-Stanovoi Complex.

Table 5 Zircon U–Pb isotopic analysis results of selected surrounding gneissose granite (sample B)

Sample	Isotopes Age/Ma												
	Th/U	$^{207}Pb/^{206}Pb$	1σ	$^{207}Pb/^{235}U$	1σ	$^{206}Pb/^{238}U$	1σ	$^{207}Pb/^{206}Pb$	1σ	$^{207}Pb/^{235}U$	1σ	$^{206}Pb/^{238}U$	1σ
S-01	1.45	192	35	357	6	383	3	0.04994	0.00074	0.42198	0.00866	0.06129	0.00042
S-02*	1.84	831	53	540	15	466	6	0.0668	0.00181	0.7015	0.02512	0.07503	0.00098
S-03	1.11	512	31	402	6	383	2	0.05753	0.00094	0.48533	0.00888	0.06128	0.00034
S-04	1.24	251	29	365	5	383	2	0.05122	0.00078	0.43233	0.00752	0.06125	0.00037
S-05	1.45	436	71	390	10	382	3	0.05559	0.00172	0.46813	0.01409	0.06108	0.00046
S-06	1.34	675	27	429	7	384	3	0.06202	0.00098	0.52555	0.00996	0.06132	0.00048
S-07	1.44	339	31	377	6	383	3	0.05324	0.00097	0.4497	0.00916	0.06127	0.00051
S-08*	2.31	490	41	386	8	368	2	0.05696	0.00121	0.46299	0.01083	0.05883	0.00037
S-09	1.37	206	37	361	6	383	2	0.05024	0.00076	0.42644	0.00902	0.06126	0.0004
S-10	1.49	180	42	357	7	383	2	0.04967	0.00076	0.42155	0.0098	0.06119	0.00039
S-11	1.38	191	38	358	8	383	5	0.0499	0.00089	0.42234	0.01158	0.06124	0.00085
S-12	1.38	286	39	371	8	383	4	0.05201	0.00086	0.44089	0.01143	0.06129	0.00067
S-13*	1.41	202	45	425	8	465	3	0.05015	0.00068	0.51954	0.01246	0.07486	0.00044
S-14	1.11	199	48	357	8	381	2	0.05009	0.00077	0.4208	0.01074	0.06096	0.00036
S-15	1.34	413	55	388	9	383	2	0.05503	0.00088	0.46503	0.01353	0.06123	0.00034
S-16	1.27	164	52	355	10	384	5	0.04933	0.00085	0.41844	0.01351	0.06137	0.00077
S-17	1.58	276	58	370	10	383	3	0.05178	0.00107	0.43913	0.01427	0.06128	0.00054
S-18	1.3	226	56	362	10	383	4	0.05068	0.00103	0.42896	0.01381	0.06123	0.0006
S-19	0.8	136	65	352	10	383	2	0.04875	0.00067	0.41498	0.01328	0.06122	0.00033
S-20	1.29	472	76	397	13	383	3	0.0565	0.00137	0.47881	0.01904	0.06128	0.00043

*means the sample is not shown in the Concordia diagram

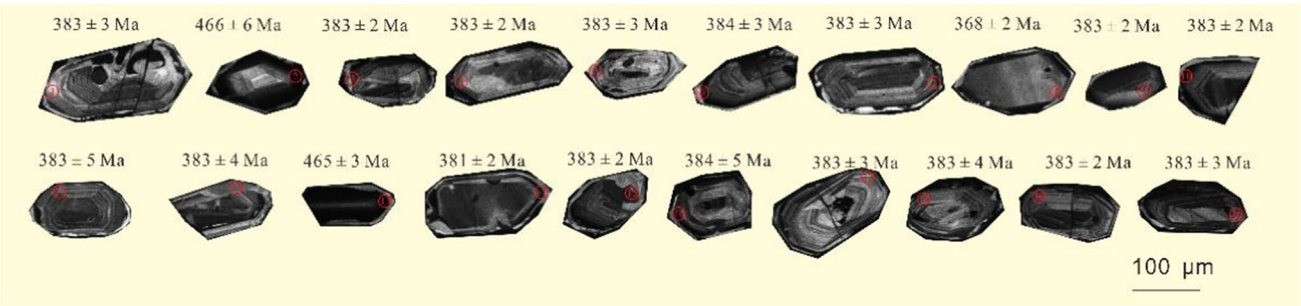

Fig. 10 Morphological and textual characterisation of zircon crystals in surrounding gneissose granite sample by CL images

The Precambrian granite gneisses was not detected or sampled in this study. The surrounding rocks of Dzhalinda intrusion are predominantly gneissose granite and granodiorite, which was estimated to be formed in stage two, with the age determined to be 382.0 ± 1.2 Ma in this study. In late Devonian period, a series of insignificant hydrothermal activity occurred, which can be identified in the rare ore free veins and lenses. The dikes of diorite porphyrites, granodiorite and granite porphyries, and spessarties might be intruded in several stages. They are found to be formed in this stage and cut the massif and surrounding rocks. The gold mineralization was considered to be confined to the southern margin of the Dzhalinda Massif and its outercontact with some Middle–Upper Jurassic sedimentary rocks.

Tectonic background and implications

The Kirovskoe deposit is located in the northern limb of the Mongol-Okhotsk suture, and its development was confined two adjacent geoblocks.

At that time of the Dzhalinda genesis, Northeast Asia was located in the double superposition and transformation of the Mongolian-Okhotsk tectonic system and the Pacific Rim tectonic system. The former is the extensional environment of the crust thinning structure following closure of

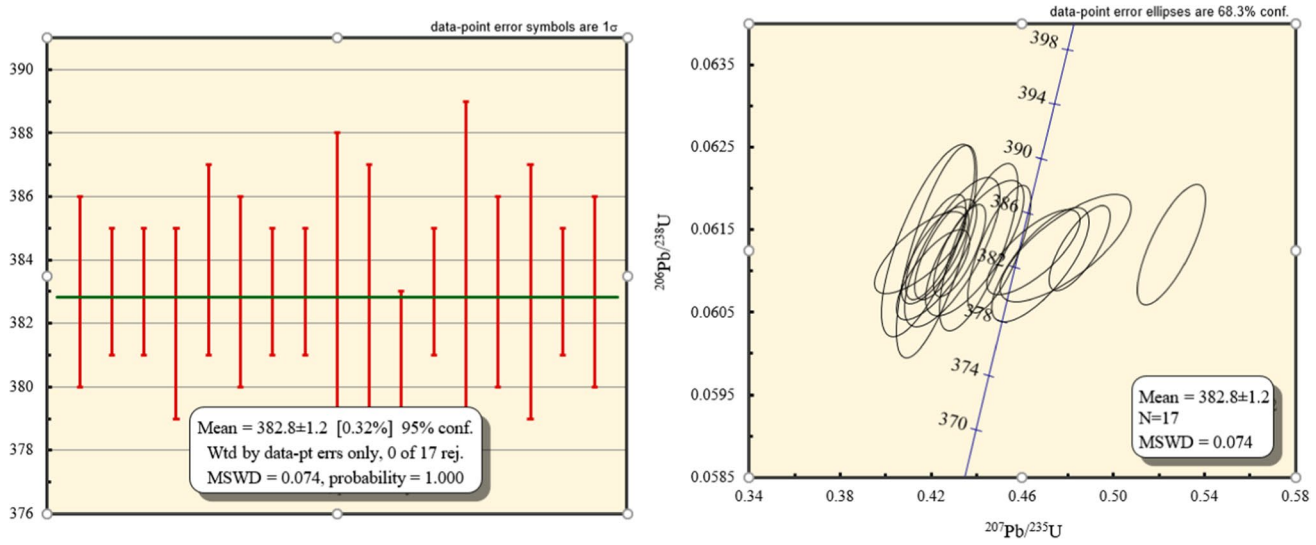

Fig. 11 Concordia diagram with U–Pb isotopic plots for zircons in surrounding gneissose granite sample

the Mongolian-Okhotsk ocean, and the latter is the paleo-Pacific Plate tectonic environment of active continental margin formed by subduction to Eurasia (Nokleberg 2005). Studies have shown that granites formed in these two different tectonic backgrounds have different rock types and geochemical characteristics (e.g., Rogers and Greenberg 1990; Zhang et al. 2008) (Table 6). Dzhalinda intrusion rocks have the characteristics of granites of the active continental margin tectonic environment under plate subduction. The Dzhalinda massif and surrounding rocks are cut by the dikes of diorite porphyrites, granodiorite and granite porphyries, and spessarties intruded in several stages. Combined with the aforementioned geochemical characteristics, the magma of the Dzhalinda intrusion may be mainly derived from the mantle wedge above the lithosphere of the young oceanic crust subduction, melted, and contaminated by crustal materials. Therefore, the Dzhalinda rock mass was formed in the Pacific Rim tectonic system, that is, the subduction of the ancient Pacific plate to the Eurasian plate.

In the Early Cretaceous, under the tectonic background of the continuous subduction of the paleo-Pacific Plate (Izenai Plate) from north-east to south-west to the Eurasian continent, the northeastern part of the Eurasian continent (including the mining area) was in a state of right-handed strike-slip stress field. This occurred at the same time that parallel secondary faults were formed by northeast-trending fault structures, and the near-east fault structures also activated and formed parallel secondary fault structures. After the Dzhalinda rock mass was in place, it was rich in Au, Ag, Cu, Pb, and other mineralizations. Following the magmatic period of elements, hydrothermal fluids along the north-east and north-west fault structures were filled and deposited from west to east, successively, so that the deposits showed different combinations of high-, medium-, and low-temperature minerals.

Conclusions

1) The rock type of the Dzhalinda intrusion is neutral diorite and belongs to the calc-alkaline series. The genetic type of the Dzhalinda intrusion body is type I. The trace elements are characterized by obvious Sr-rich and poor Yb, slightly enriched in large ion lithophile elements Rb, K, and weakly depleted high-field elements such as Nb, Ta, Zr, P, Ti. The rare-earth element distribution line is slightly tilted to the right, and there is no negative Eu anomaly. This indicates that the magma may mainly originate from the partial melting of the mantle wedge above the lithosphere where the young oceanic crust

Table 6 Types of granites formed under different tectonic settings and their main geochemical characteristics

Structure background	Sr	Yb	Eu
Crustal thinning extensional structure background	$<400\times10^{-6}$	$>2\times10^{-6}$	Negative anomaly
Active continental margin under plate subduction	$>400\times10^{-6}$	$<2\times10^{-6}$	No or weak negative anomaly
Dzhalinda intrusion (Sr, Yb mean value)	570×10^{-6}	1×10^{-6}	No negative anomaly

subducts into the ocean and is contaminated by crustal materials.

2) The Dzhalinda intrusion was formed in the Circum-Pacific tectonic system, and its genetic mechanism is the subduction of the paleo-Pacific Plate to the Eurasian continental plate. The zircon U–Pb age of the sample taken is 125.44 ± 0.69 Ma, which is the product of Early Cretaceous magmatic action. The age of surrounding rock is determined to be 382 ± 1.2 Ma.
3) The metallogenesis of the Kirovskoe gold deposit is the filling of hydrothermal fluid along the northeast and northwest fault structures following the magmatic stage of the Dzhalinda intrusion.

Author contribution All authors contributed to the study conception and design. The concept was proposed by Yanchen Yang. Material preparation, data collection, and analysis were performed by Baoyi Li and Jianpeng Wang. The first draft of the manuscript was written by Baoyi Li and Jianpeng Wang and revised by Yanchen Yang. All authors have read and approved the final manuscript.

Funding The authors would like to acknowledge the funding support from the China Geological Survey (DD20160101; 1212011120342).

Availability of data and material Original data will be available on request.

Code availability Not applicable.

Declarations

Ethics approval Not applicable.

Consent to participate Not applicable.

Consent for publication Not applicable.

Conflict of interest The authors declare no competing interests.

References

Abramov B (2012) Conditions of formations, mineralogy-geochemical features of rocks and ores of Sredne-Golgotaisk gold ore deposit (East Transbaikalia). Izv Vuzov Ser Geologija i Razvedka 3:79–82

Allaby M (2013) A dictionary of geology and earth sciences. Oxford University Press

Armstrong-Altrin JS (2020) Detrital zircon U-Pb geochronology and geochemistry of the Riachuelos and Palma Sola beach sediments, Veracruz State, Gulf of Mexico: A new insight on palaeoenvironment. J Palaeogeogr 9:1–27

Bortnikov N, Mozgova N, Nekrasov I, Rozov D, Tupyakov V, Tsepin A (1982) Particularities of bismuth mineralization in gold ores of eastern Transbaikalia. Mineral Zh 4:45–58

Boynton WV (1984) Cosmochemistry of the rare earth elements: meteorite studies, Developments in geochemistry. Elsevier, pp 63–114

Chai L, Bao Q, Zhou Y (2017) General situation and potential of diamond- precious metals in Russian Far East Federal District geological review. 63:31–32

Chppell B, White A (1992) I-and S-type granites in the Lachlan Fold Belt. Transactions of the Royal Society of Edinburgh. Earth Sciences 83:1–26

Clarke D (1981) The mineralogy of peraluminous granites; a review. Can Mineral 19:3–17

DePaolo DJ (1981) Trace element and isotopic effects of combined wallrock assimilation and fractional crystallization. Earth Planet Sci Lett 53:189–202

Gvozdev V, Goryachev N, Vakh A, Fedoseev D, Semenyak B (2013) Mineral composition of gold-bearing veins and typomorphic features of their minerals in the Kirovskoe deposit (Upper Amur region). Russ J Pac Geol 7:403–415

Gvozdev VI, Grebennikova AA, Vakh AS, Goryachev NA, Fedoseev DG (2020) Mineral evolution during formation of gold–rare-metal ores in the Sredne-Golgotay deposit (Eastern Transbaikalia). Russ J Pac Geol 14:66–86

Nasdala L, Hofmeister W, Norberg N, Martinson JM, Corfu F, Dörr W, Kamo SL, Kennedy AK, Kronz A, Reiners PW (2008) Zircon M257-a homogeneous natural reference material for the ion microprobe U-Pb analysis of zircon. Geostand Geoanal Res 32:247–265

Nokleberg WJ (2005) Metallogenesis and tectonics of the Russian far east, Alaska, and the Canadian cordillera. US Dept. of the Interior, US Geological Survey

Rogers JJ, Greenberg JK (1990) Late-orogenic, post-orogenic, and anorogenic granites: distinction by major-element and trace-element chemistry and possible origins. J Geol 98:291–309

Sláma J, Košler J, Condon DJ, Crowley JL, Gerdes A, Hanchar JM, Horstwood MS, Morris GA, Nasdala L, Norberg N (2008) Plešovice zircon—a new natural reference material for U-Pb and Hf isotopic microanalysis. Chem Geol 249:1–35

Sorokin AA, Ponomarchuk VA, Travin AV et al (2012) In Proceeding of the Second All Russian Scientific Conference on Problems of geology and complex exploration of the natural resources of the Eastern Asia, pp 57–58

Sorokin A, Ponomarchuk A, Travin A, Ponomarchuk V, Vakhtomin K (2014) New 40 Ar/39 Ar age of granitic rocks and related gold mineralization at the Kirovskoye Deposit (southeastern margin of the North Asian Craton), Doklady Earth Sciences. Springer, pp 1230–1235

Streckeisen A (1976) To each plutonic rock its proper name. Earth Sci Rev 12(1):1–33

Sun SS, McDonough WF (1989) Chemical and isotopic systematics of oceanic basalts: implications for mantle composition and processes. Geological Society, London, Special Publications 42(1):313–345

Vickers JM (1962) A critical investigation of Frank Ramsey's theory of value and belief

Vinogradov A (1962) Average contents of chemical elements in the principal types of igneous rocks of the earth's crust. Geochemistry 7:641–664

Wood D, Joron J-L, Treuil M, Norry M, Tarney J (1979) Elemental and Sr isotope variations in basic lavas from Iceland and the surrounding ocean floor. Contrib Miner Petrol 70:319–339

Yaroshevsky A (2006) Abundances of chemical elements in the Earth's crust. Geochem Int 44:48–55

Zhang Q, Wang Y, Jin W, Jia X, Li C (2008) Criteria for the recognition of pre-, syn-and post-orogenic granitic rocks. Geol Bull China 27:1–18